Measuring Molecular Adsorption on Graphitic Surfaces via Sprayed Graphene Field Effect Transistors

Tamon Raymond Page

A thesis submitted in partial fulfillment of the requirements for the degree of

Master of Science
in
Materials Science and Engineering

University of Washington

2012

Program Authorized to Offer Degree:
Materials Science and Engineering

University of Washington
Graduate School

This is to certify that I have examined this copy of a master's thesis by

Tamon Raymond Page

and have found that it is complete and satisfactory in all respects and that any and all revisions required by the final examining committee have been made.

Committee Members

_____
Marco Rolandi

_____
Xiaodong Xu

_____
Mehmet Sarikaya

Date: _____

Signature _____

Date _____

University of Washington

Abstract

Measuring Molecular Adsorption on Graphitic Surfaces
via Sprayed Graphene Field Effect Transistors

Tamon Raymond Page

Chair of the Supervisory Committee:
Professor Mehmet Sarikaya
Department of Materials Science and Engineering

The characterization of biomolecular adsorption is instrumental in applications such as biomedical implants and diagnostic devices. Graphitic surfaces such as graphene and pyrolytic graphite are prime candidates for these applications. However, a literature survey of adsorption characterization techniques shows a lack of scalable, high-throughput platforms for in-situ monitoring of biomolecular adsorption on graphitic surfaces. This thesis develops and evaluates a platform using sprayed graphene field effect transistors for in-situ tracking of biomolecular adsorption onto graphitic surfaces.

The binding affinities of graphite-binding peptides to a graphitic surface were electrically characterized using sprayed graphene field effect transistors (SGFETs) fabricated with solution exfoliated graphene. The binding affinities of these peptides were also characterized using atomic force microscopy (AFM) and mechanically exfoliated graphene field effect transistors (GFETs) to confirm the validity of the SGFET platform. Binding constants obtained via GFET and AFM were comparable with those observed using SGFETs. The sprayed graphene film serves as a scalable platform to study biomolecular adsorption to graphitic surfaces.

Table of Contents

List of Figures and Tables

Acknowledgements

Research support was provided by the NSF through the NSF-Biomaterials (DMR-0706655) and MRSEC program (DMR-0520567) at GEMSEC, Genetically Engineered Materials Science and Engineering Center, University of Washington, and the Japan Science and Technology Agency through the JST PRESTO program. The work for this thesis was carried out at the GEMSEC-SECF, a member of Materials Facilities Network of MRSEC.

Another large source of support was numerous teaching assistant appointments by the Department of Materials Science and Engineering at the University of Washington.

I would like to thank the members of my MS Supervisory Committee, Professor Mehmet Sarikaya, Assistant Professor Marco Rolandi, and Assistant Professor Xiaodong Xu for their support and guidance.

I would also like to thank my colleagues: Hilal Yazici, Emre E. Oren, Carolyn Gresswell, Dmitriy Khatayevich, Christopher So, Brandon Wilson, and Yuhei Hayamizu, all of whose help was instrumental in the progress of this research.

Introduction

Adsorption behavior of biomolecules has been an intensely studied topic over the past few decades, with many applications such as biomedical implants, biosensors and biochips for diagnosis, bioelectronics, and biomimetic materials[1]. Procedures such as joint replacement and mechanical heart valve implants are now common with approximately 773,000 Americans having joint implants in 2009[2] and over two million cases of mechanical heart valve implants in the world over the past several decades[3]. Diagnostic devices based on biomolecular adsorption and detection are in development, offering promising platforms for reliable high-throughput detection of low-abundance protein markers[4,5]. As parameters such as affinity and adsorption kinetics of the target molecule to the surface and the stability of the target molecule on the surface once it has adsorbed are all critical in the design of these applications, these applications must be supported by *in-situ* and *ex-situ* studies of biomolecular adsorption using sensing platforms such as Surface Plasmon Resonance (SPR) and Quartz Crystal Microbalance (QCM), as well as many other techniques.

Listed below are current techniques commonly used in the characterization of biomolecular adsorption. Each technique has its advantages and disadvantages, those of which are summarized in Table 1.

Standard Characterization Techniques

Surface Plasmon Resonance Spectroscopy (SPR)

Surface plasmons are propagating waves of electron density on a metal/dielectric interface (e.g. Au/glass, see Figure 1). These waves can be excited into a resonance state when an electromagnetic wave hits a metal/dielectric interface at a particular angle, absorbing energy from the electromagnetic wave. The electromagnetic field resulting from these electron density waves decay evanescently, only extending ~100nm above the metal/dielectric interface. This makes the surface plasmon resonance extremely sensitive to the surface condition of the metal, and the resonance peak will shift if the surface conditions are altered (e.g. biomolecular adsorption on the metal surface). This change can be detected in the absorption spectrum of the light reflected off of the interface, providing a platform for a highly surface sensitive sensor. The typical response time of SPR is 1~3 seconds, enabling real-time monitoring of adsorption.

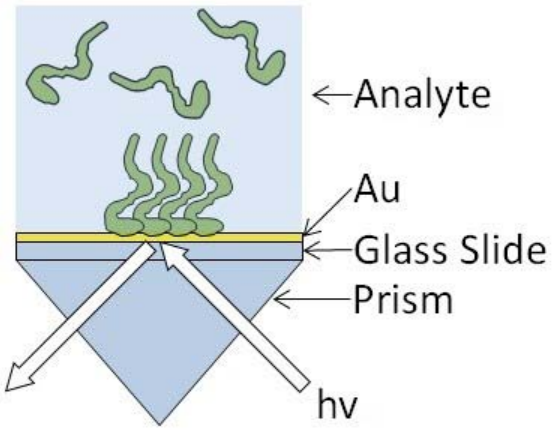

Figure 1. Cartoon representation of the experimental setup in a typical SPR sensor, and the shift in the resonance peak due to molecular adsorption on the gold surface.

A wide variety of aqueous mediums can be used in SPR, with the only limitation being that the medium doesn't adversely affect the materials used in the flow cell. Commonly used mediums include deionized water, phosphate buffer saline (PBS), phosphate/carbonate buffer (PC buffer), as well as 1% sodium dodecyl sulfate (SDS) or 5% urea solution for the rinsing of the system. Though most commonly

used mediums are near pH 7, there are also studies in which buffers ranging from pH 4 to pH 11 have been used to observe pH-dependent adsorption behavior.

The temperature at which adsorption is measured is essentially limited only by the breakdown temperature of the analyte. Although the SPR is sensitive to changes in temperature, the signal can be corrected for temperature variations by utilizing a reference channel in which no analyte is flowed. Using this method, adsorption can be characterized at any temperature between the boiling point and freezing point of the analyte.

SPR can detect molecules as small as 180 Da, making it one of the most sensitive real-time adsorption detection techniques available[6]. It has been used to detect concentrations as low as 68 ng/L of a 24kDa molecule in a recent study[7].

The surface that can be used as a detection platform is a major limitation of SPR. Surface plasmon resonance can only be observed on gold and silver surfaces. Although the gold or silver surface can be coated with a thin layer of another material (such as platinum or silica[8]), the layer must be confluent and uniform, yet thin enough to allow the surface plasmon-polariton wave to penetrate the top layer. This thickness varies from material to material, but generally cannot be thicker than 4 nm. Bulk metals such as platinum and titanium can be sputtered on to the gold to provide a testable surface, but materials such as graphite and MoS_2 in which crystallinity is critical cannot be deposited in this manner.

Quartz Crystal Microbalance (QCM)

A quartz crystal can be made to mechanically vibrate at specific frequencies because of its piezoelectric properties. Since an object's mechanical vibration resonance frequency is related to its mass and dimensions, an increase in the crystal's mass due to adsorption of biomolecules can be determined. The shear waves produced by the crystal only penetrate ~200 nm into the analyte, limiting detection to very short distances from the surface. The damping effects of liquids and gasses on the crystal are small compared to that of adsorbed solids, enabling its use with various media.

Typical media used in QCM measurements are deionized water, PBS, and PC buffer, but studies which focus on the pH dependence of adsorption characteristics may titrate acids or bases (NaOH or HCl) to reach the desired pH range of anywhere between 2.5~10.0[9].

Temperature is a limiting factor in QCM, as the most standard quartz crystal cut (the AT-cut) is only accurate at 25°C due to temperature-frequency coupling. Internal stresses caused by temperature gradients cause the resonant frequency to shift, reducing sensor accuracy. For this reason, most QCMs are outfitted with a temperature control unit which maintains the system at 25 ± 0.1 °C. The relationship between temperature and resonant frequency is cubic and has an inflection point at 25°C, which allows minor temperature fluctuations of about ±0.1°C near room temperature with negligible loss of accuracy. Stress compensated crystals (SC-cut) have an inflection point at higher temperatures (~92°C) and are less affected by temperature fluctuations, but are much more difficult to manufacture and are higher in cost.

The detection limit of QCM is traditionally an order of magnitude lower than that of SPR, and can detect the adsorption of molecules on the order of 1000 Da. However, the signal-to-noise ratio at this level of detection is low and the signal must be averaged over a timescale of 102~103 seconds for a reliable signal. This makes QCM unable to obtain reliable real-time kinetics of adsorption for small molecules, but it is still viable and widely used for equilibrium studies.

In addition to simple adsorption, QCM can also be used to measure molecular adsorbate orientation with respect to the sample using a technique called Quartz Crystal Microbalance with Dissipation Monitoring (QCM-D). This method takes advantage of the fact that vertically oriented molecules will dissipate more vibrational energy into the liquid medium than those lying flat on the substrate, and measures the energy dissipation of the crystal by pulsing a signal to the substrate and measuring how quickly the vibration is dissipated[10].

Surfaces commonly used in QCM studies include quartz, gold, titanium oxide, and hydroxyapatite, as well as polymer surfaces such as NCO-sP(EO-stat-PO) to test biocompatibility and adsorption characteristics of particular biomolecules to these surfaces. Any material deposited on the quartz crystal as a testing surface should be as rigid and mechanically stable as possible to reduce signal degradation due to dissipation. Therefore, materials such as gold and titanium dioxide which can be sputtered onto quartz in a dense film are ideal. Although testing of graphitic surfaces with QCM has been shown to be possible[11], there has been little academic activity in this area of study regarding adsorption in solution, suggesting low usability.

Adsorption Calorimetry

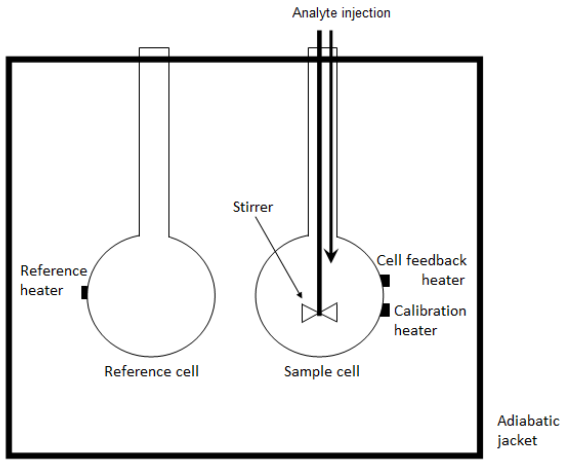

Figure 2. Cartoon of experimental setup in isothermal titration calorimetry (ITC).

Adsorption calorimetry measures the temperature change in a system due to the adsorption of a molecule of interest onto a specific surface. As the adsorption reaction takes place, heat is either absorbed or released by the reaction in accordance with the thermodynamics of the adsorption process. This enthalpy of reaction is determined by monitoring the temperature of the system, and used to calculate the thermodynamic properties of the adsorption reaction. The most commonly used calorimetry technique for characterizing biomolecular adsorption on solid surfaces is isothermal titration calorimetry (ITC). In this setup, a system of thermocouples is used to detect the temperature difference between the sample cell (filled with a liquid medium and a powder of the surface of interest) and the reference cell (filled with just the liquid medium), and a set of heaters (labeled "reference heater" and "calibration heater" in Figure 2) are used to maintain equal temperatures between the two cells. As the analyte is injected into the sample cell in precise volumes, the adsorption reaction of the ligand to the powder surface can cause a difference in the temperature of the two cells. A feedback loop corrects this difference by changing the output of the sample cell heater, and the difference in output between the reference and sample cell heaters is monitored. This yields a plot of heat evolved versus total analyte concentration, which can then be used to determine molar enthalpies of adsorption for given analyte vs. surface area ratios.

Virtually any aqueous medium may be used in this setup, provided its Hastelloy sample cells are not damaged by the medium. In the context of biomolecular adsorption, typical media include deionized water, PBS, and PC buffer. The surfaces on which analyte adsorption can be tested is also very versatile, as the material need only be available in powder form.

Typical temperature ranges studied with ITC are from 5°C to 30°C, but there have also been studies in which reactions are studied at 60°C where the proteins begin to denature[12].

Because the focus of this technique is on the characterization of the thermodynamics of the adsorption rather than monitoring the adsorption event itself, adsorption calorimetry is not used for real-time detection of molecular adsorption. Sensitivity in terms of detection limit is low, and sample volumes on the order of mL and analyte concentrations of tens of μM, two or more orders of magnitude higher than other techniques discussed in this paper, are not uncommon. The strength of adsorption calorimetry lies in that it can directly observe the enthalpy of adsorption under certain desired conditions such as temperature and solute effects, not the observation of the kinetics of the adsorption.

Enzyme-Linked Immunosorbent Assay (ELISA)

The Enzyme-Linked Immunosorbent Assay (ELISA) is commonly used in immunology to detect the presence of antigens or antibodies in a serum sample. Traditional ELISA involves the following steps (Figure 3):

1. Immobilization of antigen on a surface (e.g. a glass well)
2. Passivation of remaining surface
3. Exposure of antigen to serum (antibodies)
4. Exposure of bound antibodies to anti-antibody with linked enzyme
5. Conversion of a test chemical to a detectable form by linked enzyme (color or other signal)

There are also light rinsing steps with mild deionized water between each step outlined above to remove non-specifically bound molecules. Degree of signal obtained in final step dictates the concentration of antibodies – and therefore the immunoresponse observed – in the tested serum.

To adapt ELISA for detection of molecular adsorption on solid surfaces, an antibody must be selected for the molecule to be detected. Because of the impracticality of selecting an antibody for molecules which are already adsorbed onto a surface, ELISA is not used for the quantification of molecular adsorption on solid surfaces.

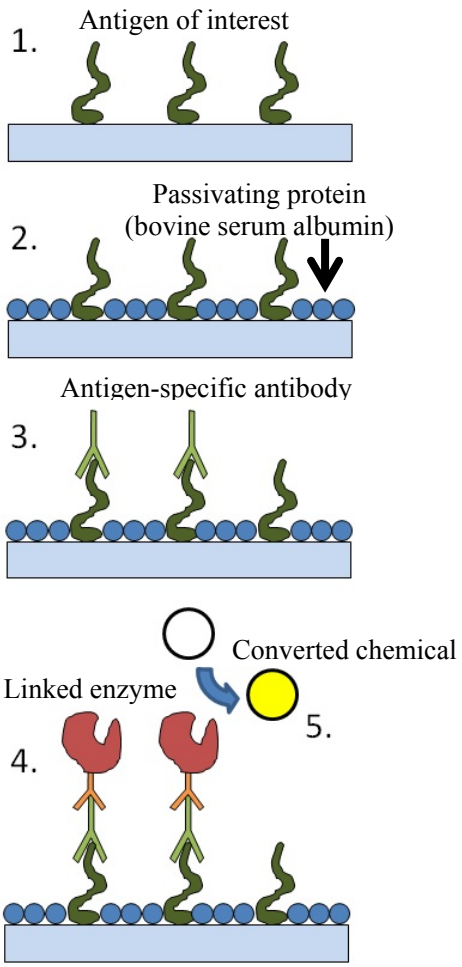

Figure 3. Cartoon of steps involved in Enzyme-Linked Immunosorbent Assay (ELISA).

Fluorescence Microscopy

Fluorescence microscopy involves the conjugation of a fluorescent dye to the molecule of interest, followed by the immobilization of this conjugate on to a solid surface. The surface is then observed under an optical microscope which has a specialized set of optical filters which limits the excitation wavelength to the wavelength specific to the fluorophore used to label the specimen and limits the observed emission wavelength to the fluorophore's emitted wavelength (Figure 4). This allows for the observation of the fluorescence signal from the fluorophore, allowing the observation of the immobilized conjugates.

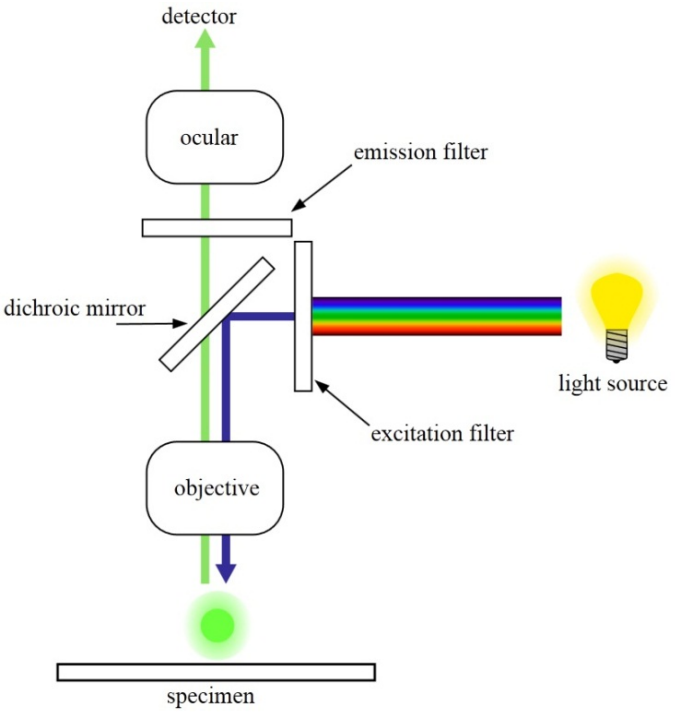

Figure 4. Cartoon of a setup for fluorescence microscopy.

This technique can observe molecular adsorption on virtually any solid, so long as the material does not display a fluorescence spectrum which overlaps with the fluorophore being used, or suppresses the fluorescence of the fluorophore. Common surfaces studied are mostly metals and oxides including gold, titanium oxide, and hydroxyapatite. Adsorption onto graphite cannot be observed using this technique, as graphite suppresses fluorescence under certain conditions[13].

The pH range of media usable with this technique is limited by the stability of the fluorophores in solution. Fluorescent proteins and quantum dots can be denatured or

dissolve and lose their fluorescence when exposed to pH extremes beyond 6~8. A line of dyes called the Alexa Fluor Dye Series claims to remain highly fluorescent over a broad pH range, but its recommended pH range is still between 6.5~8.5.

One of the biggest strengths of fluorescence microscopy is that it is an optical microscopy technique. It can provide spatial resolution on the order of 1μm, whereas most of the other techniques discussed in this paper cannot provide any spatial resolution. It is also a relatively high-throughput characterization technique, as it can be used to determine the relative adsorption of a molecule on a surface in minutes. Adsorption studies using atomic force microscopy can give even finer spatial resolution, but is inefficient when screening for tens or hundreds of potential binders.

One of the major weaknesses in this technique is that it cannot provide real-time adsorption data. Since the observation of fluorescence must be done after multiple rinsing steps to remove excess fluorophores, only a snap-shot of coverage under certain conditions such as analyte concentration and/or time of incubation can be obtained.

Atomic Force Microscopy (AFM)

Another microscopy technique which can characterize molecular adsorption onto solid surfaces is atomic force microscopy (AFM). This technique rasters a silicon tip with a nanometer-size radius of curvature over a specimen, and tracks the surface topography as a function of position. AFM has incredible vertical resolution, and can reliably detect height changes on the order of angstroms, allowing the identification of atomic features such as step edges on atomically flat single-crystalline substrates such as graphite and thermally evaporated gold. Its horizontal

resolution is on the order of nanometers, and can detect the adsorption of individual molecules on a surface. Figure 5 (on the next page) shows an example of molecular adsorption characterization using AFM[14]. Although individual molecules are not resolvable in this image, the formation of pores in the film (Figure 5D, 5E), as well the organization of the adsorbed molecules (Figure 5F) can be readily observed. Pseudo-kinetic studies can also be done using AFM, rinsing the surface after a short incubation period with analyte on the surface, allowing only the molecules bound strongly after a short period of time to be imaged. Repeating this procedure for multiple incubation times yields a plot of coverage versus time, which can then be used to determine kinetic binding coefficients. However, it is important to keep in mind that this is only a pseudo-kinetic study. The morphology and coverage on the sample may be altered by sample preparation before imaging, and may not reflect the true kinetics of the adsorption event.

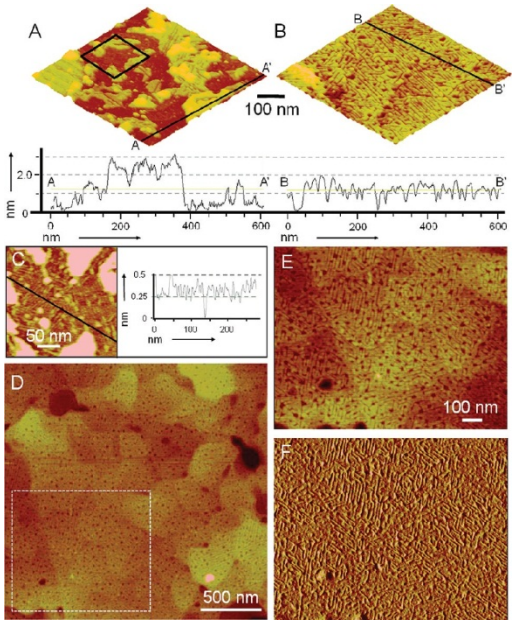

Figure 5. Example of molecular adsorption characterization using atomic force microscopy. Reproduced from So et. al, 2009.

The surfaces which can be explored using AFM are severely limited by topography. Only atomically flat surfaces can be characterized using this technique, as adsorbates can only be identified by their topography. On surfaces such as sputtered gold or optically polished glass, the topography change attributed to adsorbates will be lost in the roughness of the base sample. An RMS roughness of an order of magnitude smaller than that of the adsorbate is desirable for characterization using AFM.

Surface Resistance-Based Electrical Adsorption Measurement Techniques

A new class of biosensors based on measuring the resistivity along a semiconductive/semimetallic sensing element has recently been gaining attention. When a charged molecule adsorbs to the surface of the sensing element, it induces a charge inside the element opposite to that of the adsorbed molecule, changing the doping of the element. This change can be detected as a resistivity change along the element, and is used to track adsorption of charged molecules in real-time.

The semiconductive elements used in this technique include silicon nanowires, carbon nanotubes, and few-layer graphene, and is limited to nearly atomically-thin substrates. Since the doping is induced by surface adsorbates, only the atoms within a few atomic layers of the surface will be doped by the adsorbate. The thinner the element is, the larger the change in resistivity and the higher the signal-to-noise ratio will be.

The media used most commonly are deionized water and PBS for neutral solutions, phthalate buffer solution for acidic solutions, and borate buffer solution for basic solutions. The explorable pH range with this device is limited only by the stability of the Au/Pt electrodes and the semiconductive elements, and can probe the full range of biologically relevant pHs. This platform's stable temperature range is also very wide, and is limited only by the freezing and boiling points of the media.

The detection limit of this technique with graphene as the sensing element is 0.02 ug/ml (tracking adsorption of bovine serum albumin, 67 kDa), an order of magnitude better than that of SPR[15].

Table 1. Comparison of Reviewed Molecular Characterization Techniques.

Technique	Pros	Cons
SPR	High sensitivity, high throughput, real-time monitoring, large temperature and pH range, label-free	Surface types are limited, traditionally to Au and Ag
QCM	Can measure orientation of molecule on surface through QCM-D, label-free	Narrow temperature range, low real-time resolution, requires surface with high mechanical stability
Calorimetric	Can directly determine thermodynamics of adsorption, wide range of surfaces, label-free	Little to no real-time resolution
ELISA	High sensitivity, high throughput	Requires specific antibody, requires labeling chemistry, no real-time resolution
Fluorescence Microscopy	Spatial resolution, relatively high throughput	Some surface limitations, requires labeling chemistry, no real-time resolution
Atomic Force Microscopy	High spatial resolution, High sensitivity, large temperature and pH range, label-free	Surfaces are limited, low throughput, no real-time resolution
Electric measurement (FET)	Extremely high sensitivity, high throughput, large temperature and pH range, label-free	Surfaces limited to semiconductors, surface is grounded

Adsorption on Graphite/Graphene

Graphene has been gaining interest as a platform for applications such as biosensors and other bioelectronic devices due to its electrical properties and planar nature[16,17]. The formation of stable and uniform functional biomolecular films on graphene is still a limiting factor in the development of practical and effective biosensors. To address this challenge, it is essential to establish means for quantitative characterization of in-situ binding affinity and kinetics of biomolecules to graphene. While the traditional characterization methods introduced above such as surface plasmon resonance (SPR) spectroscopy or quartz crystal microbalance (QCM) come to mind as potential platforms, graphene field effect transistors (GFETs) offer a novel approach for the characterization of molecular adsorption to planar graphitic surfaces via electrical detection[15,18-22]. Conventional approaches, however, present practical challenges such as requiring thin, mechanically stable and confluent graphene films on macroscopic sensing elements, e.g. a quartz chip in SPR. GFET-type configurations, on the other hand, require only a continuous electrical pathway to observe in-situ adsorption kinetics to an intrinsic graphitic surface.

In this thesis, we demonstrate the sprayed graphene field effect transistor (SGFET) as a scalable sensing platform which electrically monitors the adsorption of biomolecules to an intrinsic graphitic surface.

As a calibration tool to characterize this platform, we use graphite-binding dodecapeptides (GrBPs) recently developed by our group[23,24]. These peptides have a variety of binding affinity values depending on their amino acid sequences, but all interact with the graphene surface non-covalently. One of the graphite binding peptides studied here not only exhibits high coverage and strong binding to graphite, but can also form long-range ordered assembled nanostructures[24] possibly because of its amino acid composition and molecular conformation recognizing the graphene

surface[25]. This peptide may serve as a robust biomolecular tool for further surface functionalization of the graphitic surfaces.

Of the characterization techniques introduced above, the only technique which offers real-time adsorption data on graphitic surfaces is the surface resistance-based electrical adsorption measurement techniques. The preparation of graphene and its fabrication into a sensing device will be discussed, but after the physics and characterization of graphene is briefly introduced.

Basic Graphene Physics and Characterization

Graphene is a densely packed 2-D lattice of carbon atoms (Figure 6a) with each atom bound to three other atoms through sp^2 bonds. The remaining electrons form a delocalized π-electron cloud above and below the graphene plane, creating an anisotropic material with high electronic conductivity in a 2-D plane. The E-k diagram of graphene (Figure 6b) reveals points in the six corners of the Brillouin zone at which the E-k relation is linear at low energies; this indicates an effective mass of zero[26] for electrons and holes of these particular wave vectors. An electron mobility of 200,000 $cm^2V^{-1}s^{-1}$ at a carrier density of 10^{12} cm^{-2} is theorized at room temperature, even accounting for scattering by acoustic phonons in the graphene[27,28]. Graphene is considered a semi-

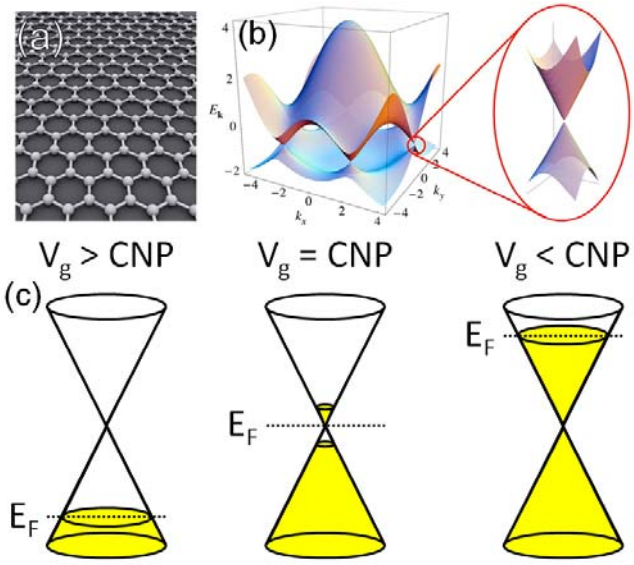

Figure 6. Graphene properties. (a) Schematic of graphene structure. (b) E-K diagram of graphene. (c) Cartoon of Fermi energy at different levels of back gate bias.

metal, with its Fermi energy lying at the boundary between the highest occupied molecular orbit (HOMO) and the lowest unoccupied molecular orbit (LUMO) as depicted in Figure 6c (middle). Imposing a gate bias on the graphene will shift this energy, injecting the sheet with holes or electrons.

In a traditional metal-oxide-semiconductor FET (MOSTFET), the transistor will have a negligible current when a gate voltage less than the onset voltage is applied, while there is no absolute "off" state in a graphene field effect transistor (GFET, Figure 7a,b). Shifting the gate voltage either way from the charge neutral point (CNP, the gate bias at which the graphene has an equal number of electrons as holes) increases the conductance of the FET, as either way the charge carrier density increases. Conduction by holes is dominant on the left side of the CNP, and conduction by electron motion is dominant on the right side of the CNP.

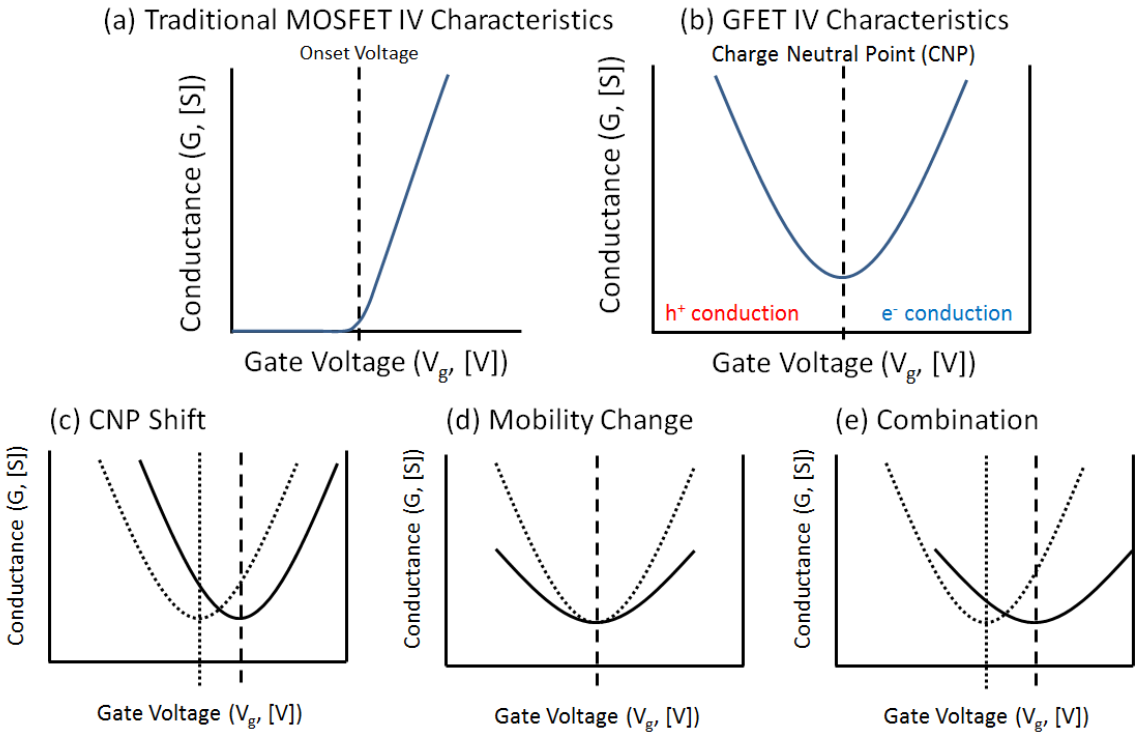

Figure 7. IV characteristics of graphene and effects of its electronic state to its IV curve. (a) Traditional MOSTFET IV curve, where the transistor turns "on" after a certain onset voltage. (b) Typical GFET IV curve with the CNP being the point of lowest conductance. (c) Effects of CNP shift on IV curve. (d) Effects of mobility change on IV curve. (e) Effects of simultaneous CNP shift and mobility change.

The IV characteristics of graphene may change in three ways: a CNP shift, a mobility change, or a combination of these (Figure 7c-e).

A CNP shift is observed as a horizontal translation of the IV curve, and may be caused by imposing a permanent gate voltage in an FET configuration or by the introduction of adsorbates onto the graphene sheet. When charged molecules adsorb onto graphene, their charge may either be directly injected into the graphene (charge injection doping) or stay in the adsorbate and induce a charge to accumulate in the graphene (capacitive doping). A mobility change is generally the result of the introduction of scattering events. This change in charge carrier mobility is observed as a change in the slope of the IV curve, and commonly occurs if there are defects or dislocations in the carbon lattice, as in the case of oxidation of the graphene surface (e.g. in graphene oxide), or charged adsorbates serving as scattering centers[27,29,30]. A combination of CNP shift and mobility change may also occur, resulting in both a translation and slope change in the IV profile.

Single-layer graphene (SLG) may be identified qualitatively through optical microscopy, as it absorbs 2.3% of incident light. It can also be identified quantitatively through the use of Raman microscopy, since the peak appearing at ~2700 cm^{-1} known as the 2D band is sensitive to the number of layers present[31] (Figure 8a,b).

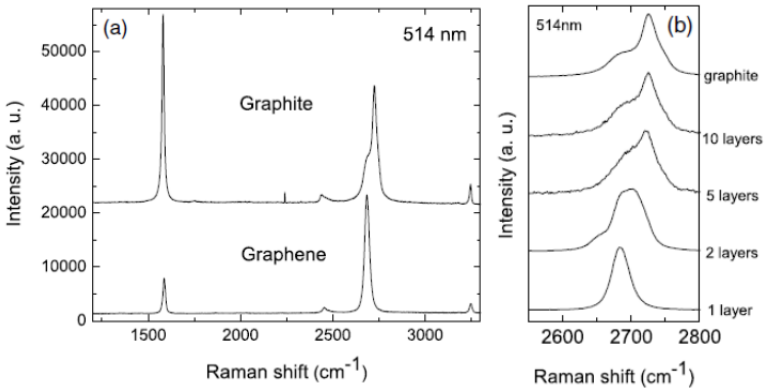

Figure 8. Raman spectrum of graphite vs. graphene using 514nm laser for excitation. (a) Overview of spectrum. (b) Detailed evolution of the 2D peak with the number of layers. Reproduced from Ferrari 2006. (Reference 31)

Now that the basics of graphene physics and characterization have been introduced, the preparation of graphene for use in GFET sensing applications will be discussed.

Preparation of Graphene for GFETs

In order to produce GFET sensors, the graphene substrate must be prepared from bulk graphite. There are four primary ways to obtain graphene: mechanical exfoliation[17], chemical vapor deposition[32], reduced graphene oxide[33-36], and liquid exfoliated graphene[37].

Mechanical Exfoliation

Mechanical exfoliation of graphene was first described in 2004 by Novoselov et al., and is achieved through the use of Scotch tape. Highly oriented pyrolytic graphite (HOPG) flakes are cleaved repeatedly with Scotch tape, after which they are transferred to a 300 nm oxide layer SiO_2 substrate through physisorption. Through chance, some of the transferred flakes will be few-layer graphene. These individual flakes of graphene can be distinguished via inspection with optical microscopy, and confirmed to be single layer graphene through Raman spectroscopy[31]. Once prepared, a GFET can be fabricated through plasma etching (See Figure 9 above) and electron beam lithography (EBL).

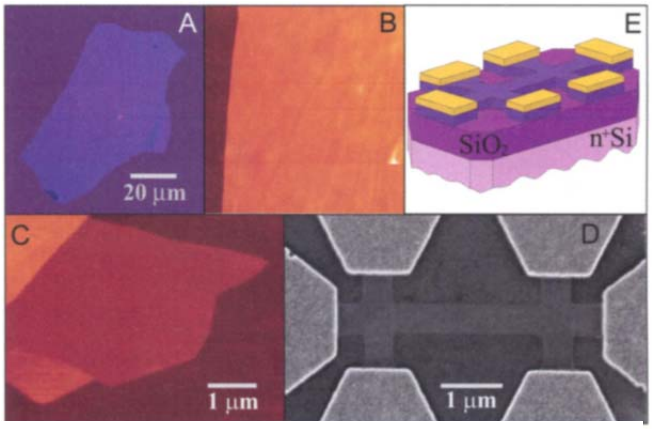

Figure 9. Mechanically exfoliated graphene. (a) as-cleaved multi-layer graphene. (b) AFM of (a). (c) AFM of single-layer graphene. (d) SEM image of an experimental graphene device. (e) schematic of device from (d). Reproduced from Novoselov et al. 2004. (Reference 17)

Chemical Vapor Deposition (CVD)

Chemical vapor deposition of graphene is the deposition of carbon from chemical vapors such as methane[32] and ethylene[38] onto a smooth substrate, usually copper[39] or nickel[32] films. This can be carried out in conditions ranging from ultra-high vacuum (UHV) to atmospheric pressures, but either way in very carefully controlled carbon source concentrations. In one example of CVD, the polycrystalline Ni substrate is heated (900-1000°C) and exposed to the carbon source, then cooled to allow the carbon to precipitate out onto the substrate surface and form single- to few-layer graphene. The formed large-area graphene may then be used to fabricate devices as with mechanically exfoliated graphene. A sample of CVD graphene transferred on to a SiO_2/Si substrate is shown in Figure 10.

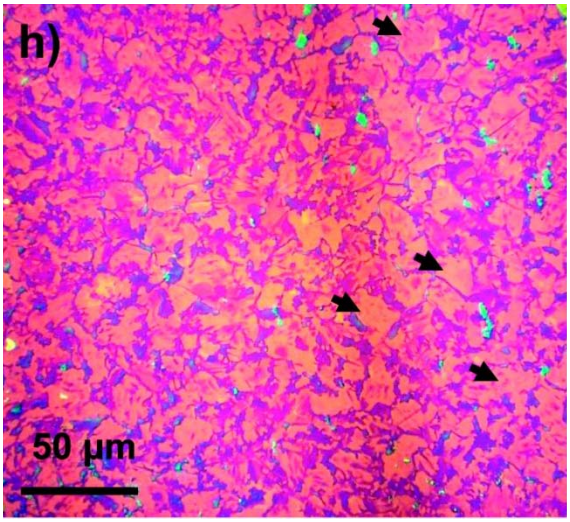

Figure 10. Optical image of CV deposited graphene grown on polycrystalline Ni and transferred to a SiO_2/Si substrate. Reproduced from Reina 2009. (Reference 32)

Reduced Graphene Oxide (RGO)

Reduced graphene oxide is commonly prepared through the Hummers method[40], chemically reacting the basal plane carbon atoms of bulk graphite with a mixture of sulfuric acid, sodium nitrate, and potassium permanganate to form epoxide and hydroxyl groups on the surface of individual graphene sheets in the bulk graphite to impart hydrophilic character and promoting complete exfoliation of single layers in aqueous media through soft sonication[33]. The oxidized graphene is deposited onto

the substrate of choice, and then reduced using hydrazine solution or hydrogen plasma. The resulting films of graphene (shown in Figure 11a above) show similar IV characteristics (seen in Figure 11b) as pristine mechanically exfoliated graphene, albeit with a conductivity that is smaller than pristine graphene by 3 orders of magnitude[33].

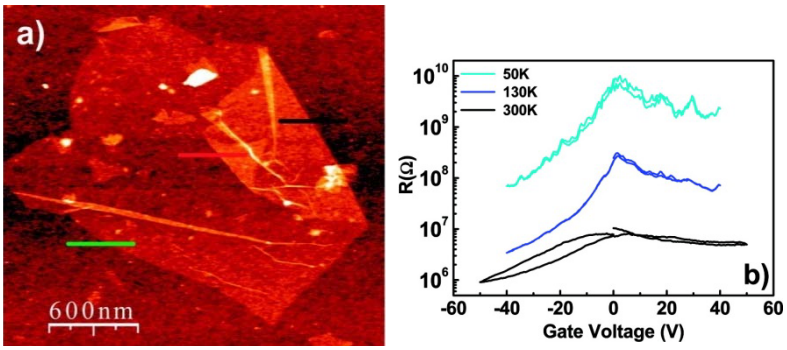

Figure 11. Reduced Graphene Oxide. (a) AFM image of a GO monolayer deposited on a SiO_2 sub-strate, showing a back-folded edge. (b) Low-bias resistance of a fully reduced GO monolayer measured as a function of back gate voltage at three different temperatures (Vbias = ±100 mV). Reproduced from Gomez 2007. (Reference 33)

Solution Exfoliated Graphene

Solution exfoliated graphene is prepared by mechanically exfoliating bulk graphite (in flake or powder form) directly in a solvent without first undergoing an oxidization step. The bulk graphite (flake or powder) is immersed in a medium with a similar solvent energy as graphene (e.g. N-methyl-pyrrolidone)[37,41], and then subjected to sonication and centrifugation to exfoliate and remove larger pieces of graphite from the solution. When this solution is spray-coated onto a SiO_2/Si substrate, it retains its IVg response, hence its viability as a sensing substrate (see Figure 12).

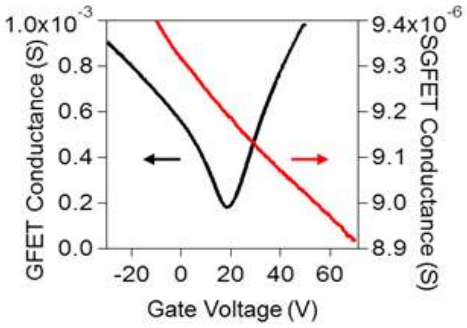

Figure 12. IV response of a GFET fabricating using a sprayed film of solution exfoliated graphene. Black trace is mechanically exfoliated, and red trace is sprayed graphene. Reproduced from Page 2012. (Reference 42)

Approach

As the goal of this work was to develop a scalable platform which can obtain kinetic information on biomolecular adsorption to graphitic surfaces and the demonstration of this platform as a viable sensor to determine binding constants for adsorbates onto graphitic surfaces, a surface resistance-based electrical adsorption measurement system with dimensional control of graphene placement is necessary to allow the fabrication of standardized device substrates (as in SPR and QCM), while preserving the quality of the graphene surface. Liquid-phase exfoliation was found to be a viable platform with which to provide flat graphitic surfaces with similar adsorption profiles to that of HOPG[42].

Device Preparation and Characterization

Sprayed graphene field effect transistor (SGFET) sensing substrates were prepared by first sputter coating Ti/Pt (2nm/50nm, Gatan Model 682 PECS) electrodes on the silicon substrates through a mechanical mask. This substrate was then heated to ~350°C using a hotplate, and an exfoliated graphene solution was sprayed on the substrate through another mechanical mask (Figure 13a, next page). Solution exfoliated graphene was prepared follows: 30mg of graphite powder was rinsed and sonicated for five minutes with acetone, dried via vacuum filtering with a 0.2 μm filter, sonicated in 30ml NMP for one hour, then centrifuged at 4000 rpm (~2000xg, Sorvall RC 5B Plus SLA-1500 rotor) for 8 hours. The top 20 ml of exfoliated graphite solution was extracted for spray coating. To eliminate any surface contamination, the prepared substrate was annealed according to literature[43] at 450°C for one hour under a flow of 40% H2, 60% Ar. A completed SGFET substrate is shown in Figure 13b (next page).

The sprayed film was characterized using Raman microscopy (Renishaw Raman Microscope at 514 nm excitation wavelength), and the apparent gate response of the film was probed using an Agilent U2722A USB Modular Source Measure Unit with a current source of 5µA and a 4-probe setup (simplified circuit diagram in Figure 13a, right, and resulting IV curve shown in Figure 12). The topography of the film was observed using a Digital Instruments Multimode AFM under tapping mode.

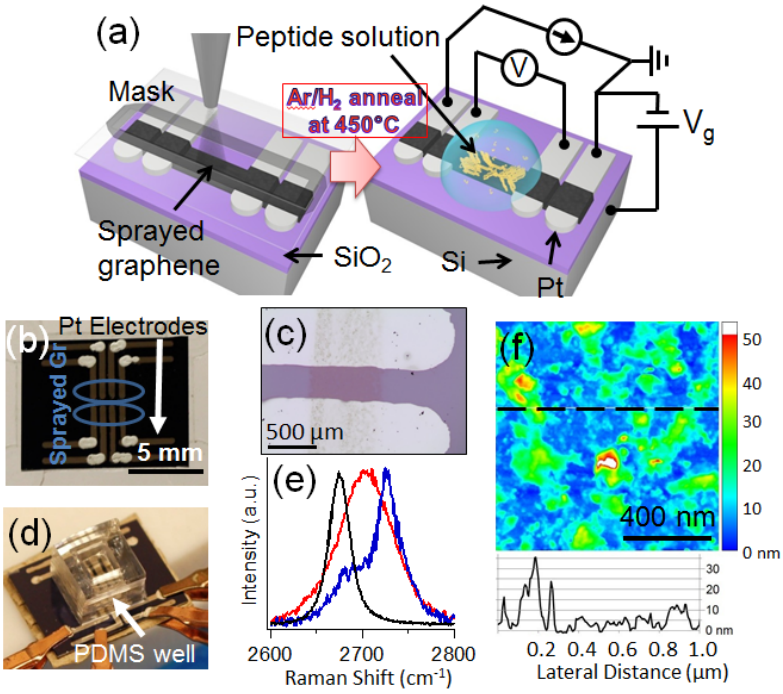

Figure 13. SGFET device preparation and characterization. (a) Schematic of SGFET device preparation. Deposit Pt electrodes and spray dispersed graphene solution. After H2/Ar, anneal, device is ready for exposure to analyte. (b) Image of sprayed graphene field effect transistor (SGFET) substrate. White blots on electrodes are Ag paste for better electrical contact. (c) Image of experimental setup using SGFET substrate. (d) Optical micrograph of graphene field effect transistor (GFET). (e) Raman spectrum of graphene (black), SGFET sensing element (red), and bulk graphite (blue). (f) AFM of sprayed film. Light blue portions denote 2-5nm multilayer graphene. Reproduced from Page 2012. (Reference 42)

The experimental configuration of the SGFET sensing substrate is shown in Figure 13d, a 4-probe setup with analyte being retained on the surface using a PDMS well. The GFET resistance was monitored using a 2-probe setup with the Agilent U2722A system, also using a PDMS well. The adsorption of two peptides, GrBP4 and GrBP5 was observed using these systems. The adsorption behavior of bovine serum albumin (BSA) was also observed as a positive control, as it is known to produce resistivity change in a similar system (Ohno et al. 2009). Before exposing to peptide solution, each substrate was equilibrated in deionized water for 30 minutes while monitoring its resistance. After equilibration, analyte (GrBP5, GrBP4, or BSA) was added in increasing concentrations to bring the total concentration to

the desired level. With GrBP5 and BSA, the analyte concentration was increased incrementally from 0.1 μM to 3.0 μM. In the case of GrBP4, the concentrations were increased from 1 μM to 10 μM to allow for reasonable equilibration times.

Correlation with Conventional GFET

Mechanically exfoliated graphene[17] was used to fabricate conventional GFETs for comparison to SGFETs. Indium microsoldering[44] was used for electrode deposition in place of lithographic processes to preserve the cleanliness of the graphene surface. A representative IV response of this GFET is shown in Figure 12. The experimental conditions for these GFETs was identical to that of the SGFETs described above.

Correlation with AFM

To complement the SGFET results, biomolecular binding affinity was also characterized by atomic force microscopy imaging (AFM) to observe surface coverage of peptides on graphite with various incubation concentrations (0.1 μM to 5 μM). The samples were prepared by mechanically exfoliating graphite flakes on a silicon substrate, incubating these flakes in various concentrations of analyte solutions for 3 hours in a humid environmental chamber (>90%), and then blowing the surface with N2. These samples were immediately imaged using a Digital Instruments Nanoscope-IIIa Multimode AFM under tapping mode, with a scan speed of 5.00 μm/sec and target amplitude of 2.00 V.

Based on the observed resistances at equilibrium, the binding affinity of each peptide was determined using the following form of the Langmuir adsorption isotherm

$$\frac{C_{analyte}}{\Delta R_{ads}} = \frac{1}{\Delta R_{max}} * C_{analyte} + \frac{1}{\Delta R_{max}} * \frac{1}{\mathrm{K_{eq}}'}$$

where $C_{analyte}$ is the concentration of the analyte solution, ΔR_{ads} is the equilibrium resistance shift observed for a given $C_{analyte}$, ΔR_{max} is the resistance shift at full coverage, and K_{eq}' is the apparent equilibrium constant*. Since $C_{analyte}$ and ΔR_{ads} are known from experiment, one can determine ΔR_{max} and K_{eq}' through this formula. As there was no practical method of determining relative surface coverage of adsorbates, ΔR_{max} was used as a normalizing factor to compare between different runs, assuming that all adsorbates would attain full coverage at high enough concentrations. K_{eq}' was determined by multiplying the above equation through by ΔR_{max}, plotting

$$\frac{C_{analyte} * \Delta R_{max}}{\Delta R_{ads}} = C_{analyte} + \frac{1}{K_{eq}'} \text{ (Fig. 17b),}$$

and determining the inverse of the y-intercept for each data set. Standard error of K_{eq}' was determined through calculating K_{eq}' using equilibrium resistance values ±1 standard deviation from the observed equilibrium resistance for each analyte and testing platform.

* Though we use the Langmuir model to explore and compare our adsorbates for convenience, it is important to note that the value we arrive at is not strictly a Langmuir equilibrium constant. Because BSA and peptides are not expected to bind reversibly to the graphene surface, we cannot follow the Langmuir assumptions, so it would be misleading to refer to the comparison factor as K_{eq}. Therefore, we adopt K_{eq}' as our factor for comparing relative adsorption strengths between the adsorbate and the graphene, which we refer to as the "apparent equilibrium constant".

Results and Discussion

Characterization of Deposited Film

The quality of the sprayed film was characterized using Raman spectroscopy and AFM. Raman spectroscopy can be used to quickly determine the quality of graphene via the 2D band in the spectrum[31]. The Raman peak of our sprayed film is located between the peaks for mechanically exfoliated graphene and bulk graphite (Figure 13e). Since the 2D peak in our spectrum does not have the characteristic shoulder seen in 5+ layer graphite, we assume the dominant flake thickness is approximately 2-4 graphene layers. AFM images of the film show the thickness ranged approximately from 0-50 nm, with regions of ~5 nm (blue to light blue in Figure 13f) and thicker 10-30 nm regions (turquoise to light green on Figure 13f). Though the conductive film as a whole is a composite of aggregated graphene and few-layer graphene flakes, enough portions along the conductive path are of few-layer graphene for these regions to dominate the electrical resistivity across the film and allow the observance of a gate response, as will be seen below.

The gate response of the SGFET and GFET were observed. Figure 12 shows the gate response for a GFET (black) and our sprayed graphene film (red). Although much shallower than that of the GFET, the sprayed film exhibited sensitivity to an applied gate voltage, allowing it to detect a resistance change due to surface adsorption.

Biomolecular Adsorption

GrBP and BSA adsorption was observed using our SGFET platform. Contrary to previous literature on GFETs[15], the resistivity increased as analyte concentration was increased, and equilibrium was usually reached within an hour (Figure 14a). The difference in resistance shift between our results and those observed in literature most likely stems from tracking conductance at different sides of the charge-neutral point (CNP). Ohno et al. tracked device conductance using Vtg = -0.1V (Vtg < CNP) and observed an increase in conductance, indicating a positive shift in the CNP or a decrease of carrier mobility. If one were to track device conductance at Vtg > CNP, it would decrease from the same IVtg profile response to BSA adsorption. Although we currently cannot confirm this hypothesis since due

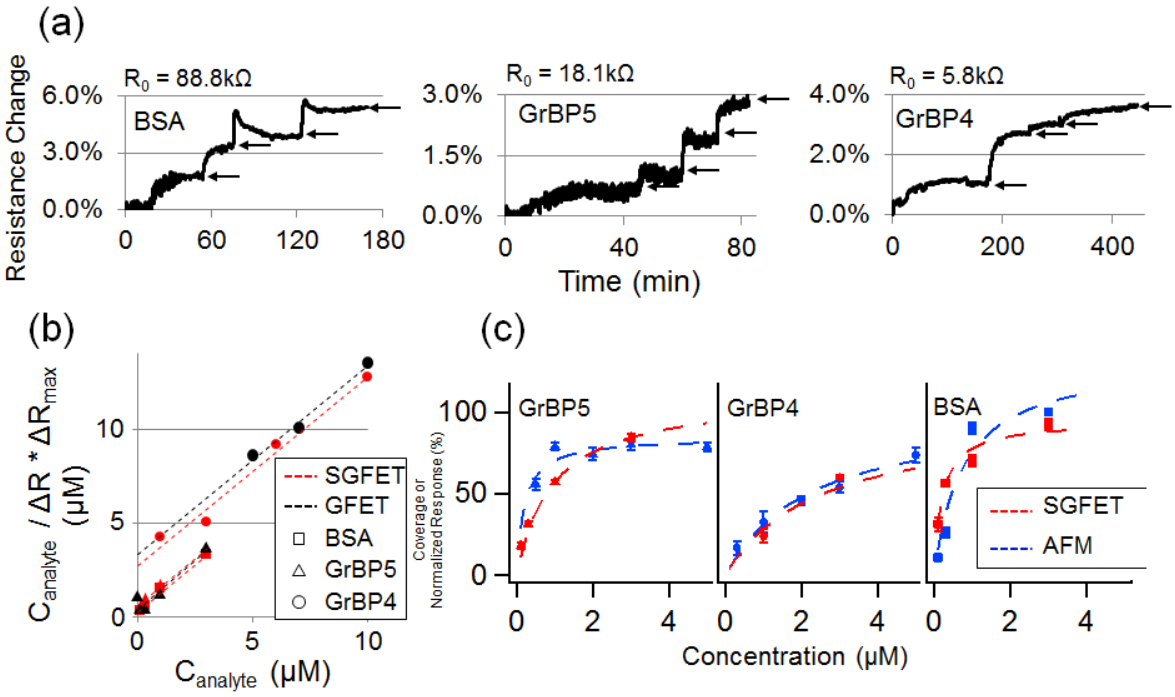

Figure 14. Adsorption measurements with SGFET. (a) Response of a sprayed GFET (SGFET) to biomolecules of varying affinity to a graphitic surface. (b) Langmuir plot comparison of SGFET response to that on a conventional GFET. Black trace is GFET using mechanically exfoliated graphene, and red trace is GFET using liquid-exfoliated graphene. (c) Langmuir plot comparison of SGFET response to adsorption on HOPG observed by AFM. Blue trace is AFM data, and red trace is SGFET. Reproduced from Page 2012. (Reference 42)

to the lack of a reference electrode to probe our devices' IVtg profiles, we plan to include the addition of a reference electrode to the list of future improvements to the system in order to allow the elucidation of this phenomenon.
The apparent equilibrium constants obtained from these studies were $0.8 \pm 0.3\ \mu M^{-1}$ for GrBP5, $0.4 \pm 0.1\ \mu M^{-1}$ for GrBP4, and $3.6 \pm 0.2\ \mu M^{-1}$ for BSA. These results support our original selection in GrBP5 being a stronger graphite binder than GrBP4, but we also observe that it is a weaker binder than the non-specifically adsorbing and more massive BSA.

Correlation with Conventional GFET

Adsorption of GrBP5 was also observed using GFETs to confirm the measurements obtained by our sprayed graphene sensing platform under the same aqueous conditions. Again, contrary to the previous literature[15], the resistivity increased as analyte concentration was increased. The apparent equilibrium constants obtained through GFET adsorption measurements were $5.4 \pm 2.1\ \mu M^{-1}$ for GrBP5 and $0.3 \pm 0.1\ \mu M^{-1}$ for GrBP4. These values illustrated good agreement with the SGFET values. The equilibrium results from GFET and the sprayed graphene sensor were plotted in Figure 14b, showing good agreement between the two adsorption characterization techniques. Since the affinity of the peptides to mechanically exfoliated graphene was similar to that on the in-solution exfoliated graphene, it can be concluded that our sprayed graphene sensor acts similarly to GFET, regardless of our platform's larger number of interconnections and edges. These results also suggest that our sprayed graphene substrates are clean enough to obtain a clear adsorption signal, much like a mechanically exfoliated GFETs.

Correlation with AFM

Figure 14c compares the actual coverage obtained through AFM to the normalized response obtained through SGFET. Each measurement is close to that obtained with the novel platform, with the most discrepancy being from BSA. A potential source of discrepancy can be seen in the line profile of the 1.0 µM and 3.0 µM BSA samples in Figure 15 (bottom): these profiles show the partial formation of adlayers (4 nm thick regions, as opposed to the discrete 2 nm features observed at low concentration). Coverage in an AFM study is only recognized as the regions of graphite that are occupied by analyte molecules, and does not take adlayer molecules into account. In SGFET, adlayer molecules may contribute to the doping of the sprayed graphene layer, resulting in a higher-than-expected "full coverage" value. This difference in detection may be responsible for the higher discrepancy between AFM and SGFET for BSA adsorption, particularly as adlayer formation is not observed for GrBP4 or GrBP5. However, the AFM results still confirm the relative K_{eq}'s of the peptides obtained with the other two sensing platforms, with apparent binding constants of 2.23 μM^{-1} for GrBP5, 0.49 μM^{-1} for GrBP4, and 1.21 μM^{-1} for BSA.

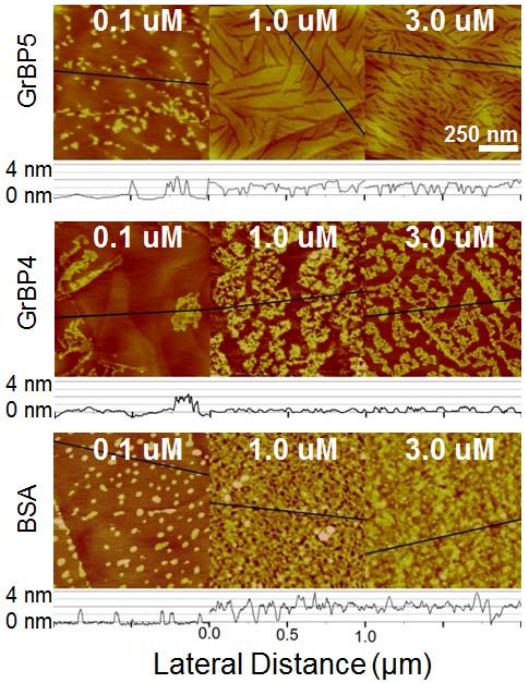

Figure 15. AFM images of surface morphology on HOPG at equilibrium for each concentration. Reproduced from Page 2012. (Reference 42)

Device Linearity

Our platform's response appears approximately linear, with good correlation between signal vs. coverage (Figure 14c), particularly for GrBP4, but there are slight discrepancies in the device linearity when detecting GrBP5 and BSA adsorption. In order to have a linear range with an FET sensor, a constant mobility and linearly shifting CNP at the increase of charge density due to adsorbate doping is necessary. Although each analyte seems to roughly fit a linear trend when comparing resistivity change to actual coverage, a slight difference in tendencies between the correlation of resistivity change and coverage is noticed in the adsorption BSA and GrBP5. This could be the result of, for example, not having a proper statistically significant analysis of the system, but it could also be due to the non-linearity intrinsic in the system unique to each adsorbate. Adsorption of peptides and proteins could affect both charge carrier mobility and CNP differently resulting from the coverage, conformation, and surface morphology of the adsorbed species, as the charged regions of the adsorbate may arrange themselves differently and act as scattering centers or simply increase the carrier charge density. To fully understand FET sensors' response to an analyte, in-depth analysis of various aspects of the adsorbate's doping effect for each condition would be required, such as doped charge density per molecule, impact on charge mobility, location of peptide binding, edge vs. planar adsorption regions[45], etc. Because of these factors, FET sensing is an interesting and complex research topic, and is surely a subject which must be discussed in detail before FET sensing platforms can come to be widely accepted. We believe, therefore, that the current goal of this thesis, i.e., the demonstration of our platform as a viable sensor to determine binding constants for adsorbates onto graphitic surfaces, has been achieved without detailed discussion of this complex issue. We leave this as question to be addressed in a future work, as the scope of such a project would be outside the frame of this thesis.

Device Reproducibility and Stability

Reproducibility was quantitatively assessed through four repeats of GrBP5 adsorption with good correlation (Figure 16a). Our devices displayed a stable signal when exposed to deionized water, as well as deionized water under a flow rate of 80 µl/min., a flow rate comparable to molecular adsorption characterization tools such as SPR.

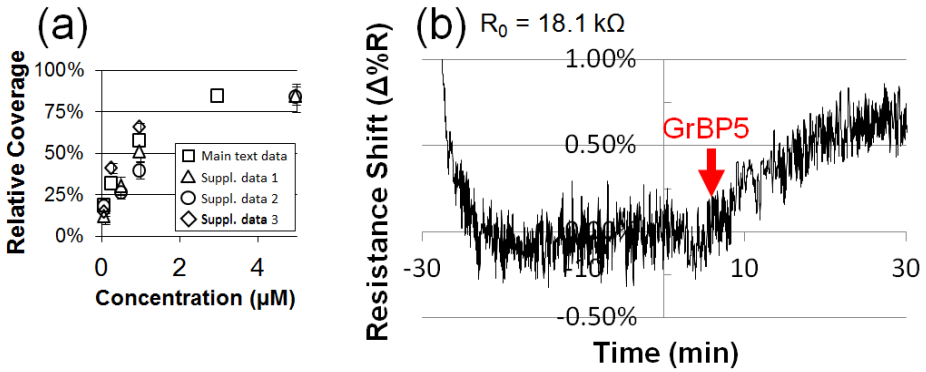

Figure 16. Device reproducibility and stability. (a) Response of our SGFET devices for GrBP5 adsorption over four different sets of adsorption data. (b) Signal during equilibration of the substrate used for Fig. 17a GrBP5 adsorption, as well as the first 30 min. of the test. The resistance of the device used in Fig. S2a was at ~18% in air. When exposed to water, the resistance rapidly decreases and reachs a pseudo-stable state. Reproduced from Page 2012. (Reference 42)

Device stability in water was evaluated from data acquired during equilibration of the device before introducing the biomolecule to the device. Figure 16b shows the signal during equilibration of the substrate used for Figure 17a GrBP5 adsorption, as well as the first 30 min. of the test. The resistance of the device used in Figure 16b was at ~18% in air. When exposed to water, the resistance rapidly decreases and reaches a pseudo-stable state.

Because the signal over time in the raw data of Figure 16b has a slight drift, a linear fit was made to define a baseline value of 0%. In this particular case, the baseline

slope was -0.024 Δ%R/min. (-4.3 Ω/min.). This was the only data set in Figure 16a with a large enough signal drift observed to warrant a slope adjustment. After equilibration and slope adjustment, the signal can be seen to be fluctuating around ±0.2% resistance shift for ~25 minutes before the analyte is injected. Conventional graphene sensors in literature have been shown to have a stable baseline for 5-10 minutes before the analyte is introduced, and we believe our platform is of a similar stability. From the above explanation, we conclude that the device is sufficiently stable in the absence of adsorbates.

Device Sensitivity

The sensitivity of our platform was higher than that of conventional GFET biomolecular sensors when compared per device, but was far lower when the sensor surface area was taken into account. Device sensitivity was first calculated as the change in resistivity versus adsorbate binding per molecule on the sensor (calculated based on Langmuir Isotherm model), then scaled according to sensor surface area. To compare the sensitivity of these platforms on a per-molecule basis, the footprint of the molecule adsorbed on the surface and the surface area of the sensors must be considered. To estimate the sensitivity of our platform relative to that of conventional GFET sensors, we make the following simple assumptions: the volume of BSA is unchanged from that in solution (~244 nm^3)[46] and the molecule deforms on to the hydrophobic surface with a height of ~1.5 nm (observation from AFM sections in Figure 15, also supported in literature[47]), therefore its adsorption footprint would be ~160 nm^2/molecule. Also assuming complete device linearity, the resistance shift of 1.80% from 0.1 μM BSA on the SGFET device from Figure 14a translates to a 31.5% coverage, or ~2000 BSA molecules/μm^2, which makes the resistance shift per BSA molecule/μm^2 approximately 0.0009%dR. For the same adsorbate detected on a GFET device in literature, the resistance shift was 1.81% at 0.12 μM BSA[15], translating to a 76.2% coverage or ~4850 molecules/μm^2, and

resistance shift per molecule/μm^2 of approximately 0.0004%. Thus from the standpoint of per-device signal per molecule/μm^2, the SGFET platform is more sensitive than a conventional GFET sensor in literature. (Non-linearity of the adsorbate detection due to its effects on the IV_{tg} profile of the FET sensor is assumed to be equal in both the conventional GFET and SGFET platforms, and is thus not considered.)

To properly compare the sensitivity of the platforms themselves and not the devices, we must normalize for sensing surface area. From this, the sensitivity of the conventional FET in literature was calculated to be $4.0*10^{-5}$ % resistance shift per BSA molecule, compared to $3.0*10^{-9}$ % per molecule with the SGFET platform, a ~13,000-fold difference. With a noise level of 0.2% dR and hence a limit of detection of 0.6% dR, the molecular limit of detection for BSA on the SGFET platform would be ~$2.0*10^{8}$ adsorbed BSA molecules, while the GFET sensor could detect ~$7.6*10^{3}$ adsorbed molecules.

Thus conventional GFETs would be far superior in sensitivity per area, but the SGFET platform is a strong competitor for determining adsorption constants of biomolecules when considering per-device sensitivity and scalability. When SGFET is used to determine adsorption constants of a large number of analytes, the scalability of the platform is expected to more than compensate for its low per-molecule sensitivity. The area-normalized sensitivity of SGFET is limited in part by its unoptimized surface conditions; the regions which are covered by multi-layer graphene are not sensitive to molecular adsorption, and the uncovered regions are also not contributing to the observed signal. With further optimization, its per-area sensitivity may be improved.

Device Stability under Flow

Next, the stability of the device under flow was considered. Of the data sets introduced in Figure 16, Supplemental Data 1 and 2 were obtained using a flow cell setup. The prototype flow cell was constructed from PDMS, and achieved an air-tight seal with the SiO2 substrate by being pressed together with an acrylic casing (setup shown in Figure 17a.

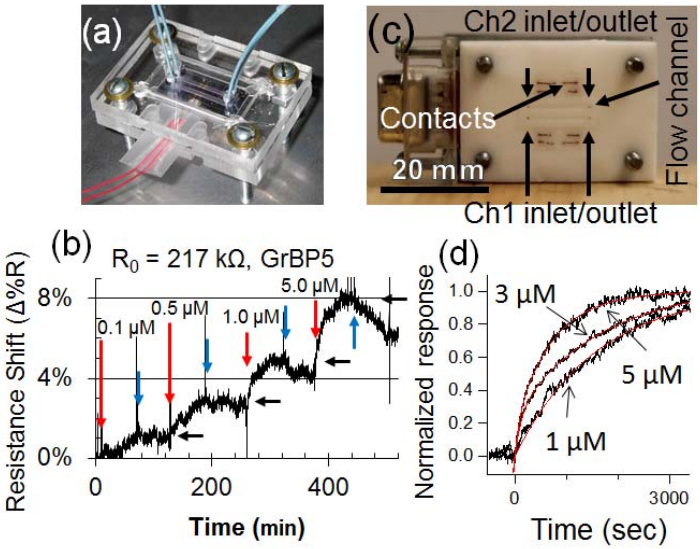

Figure 17. Device stability under flow. (a) Proto-type flow cell model. (b) Flow cell designed for standardized device substrates. (c) Adsorption curve for GrBP5 in prototype flow cell. (d) Adsorption curve for GrBP5 in improved flow cell. Reproduced from Page 2012. (Reference 42)

The analyte flow rate was approximately 80 µl/min., similar to flow rates of other analytical adsorption tools such as surface plasmon resonance (SPR) and quartz crystal microbalance (QCM). The adsorption profile for Supplemental Data 1 (from Figure 16a) is shown in Figure 17b. The observed near-equilibrium coverage is very similar to that in the main text, as seen in Figure 16a, regardless of the fact that these runs have rinsing steps (blue arrows) between each adsorption step (red arrows). The baseline is sufficiently stable over the course of 8 hours without slope adjustment. From these results, we conclude that the device is sufficiently stable under flow conditions.

Future Work

Objectives for future work include the development of a technique to more accurately measure the effect of adsorbates on the electronic structure of graphene films as well as probe the ionic permeability of adsorbate films. This and supporting data from other adsorption characterization methods such as AFM and GFET will provide more insight into the surface structure – and therefore self-assembly mechanisms – of genetically engineered peptides for inorganics. For this, the development of a graphene quantum capacitance sensor is suggested.

Conclusion

In conclusion, the binding characteristics of the peptides obtained using this platform were consistent with that obtained using two other platforms: AFM coverage analysis and GFET sensors, confirming the viability of the novel platform. The experiments carried out using the SGFET platform should also be possible using other single-layer materials such as MoS_2 and WS_2 through the preparation of the respective single-layer solutions discussed in previous literature[48].

The experiments in this study were carried out with peptides in deionized water and with no counter electrode in order to simulate the conditions used in the initial selection of the peptides. To better control environmental conditions such as surface potential, electrochemical systems typically employ reference and counter electrodes, and a buffer to stabilize solution conditions. Further studies should investigate these factors to establish more stable measurement of molecular adsorption. Under a better-controlled environment, kinetic constants of biomolecular adsorption such as deposition rate and sticking coefficient can also be evaluated[49].

The GrBPs examined here are part of a molecular toolset called genetically engineered peptides for inorganics (GEPIs)[50]. This toolset offers a host of peptides which selectively bind to a wide variety of different materials (metals, oxides, minerals, etc.), a number of which have been used in literature as a viable platform for the immobilization of functional proteins to solid surfaces[51-53]. The expansion of this toolset to graphitic surfaces, with possibilities to other single-layer materials, opens up new possibilities of quantitative functionalization of multi-material substrates.

References

1 Kasemo, B. Biological surface science. *Surface Science* **500**, 656-677 (2002).

2 *Joint Replacement Surgery and You*, <http://www.niams.nih.gov/health_info/joint_replacement/default.asp> (

3 *Artificial Heart Valve - Encyclopedia.com*, <http://www.encyclopedia.com/topic/Artificial_Heart_Valve.aspx> (

4 Cheng, M. M. C. *et al.* Nanotechnologies for biomolecular detection and medical diagnostics. *Curr Opin Chem Biol* **10**, 11-19, doi:DOI 10.1016/j.cbpa.2006.01.006 (2006).

5 Shao, Y. Y. *et al.* Graphene Based Electrochemical Sensors and Biosensors: A Review. *Electroanalysis* **22**, 1027-1036, doi:DOI 10.1002/elan.200900571 (2010).

6 Karlsson, R. & Stahlberg, R. Surface-Plasmon Resonance Detection and Multispot Sensing for Direct Monitoring of Interactions Involving Low-Molecular-Weight Analytes and for Determination of Low Affinities. *Anal Biochem* **228**, 274-280 (1995).

7 Kwon, Y. C. *et al.* Development of a surface plasmon resonance-based immunosensor for the rapid detection of cardiac troponin I. *Biotechnol Lett* **33**, 921-927, doi:DOI 10.1007/s10529-010-0509-0 (2011).

8 Seker, U. O. S., Wilson, B., Sahin, D., Tamerler, C. & Sarikaya, M. Quantitative Affinity of Genetically Engineered Repeating Polypeptides to Inorganic Surfaces. *Biomacromolecules* **10**, 250-257, doi:Doi 10.1021/Bm8009895 (2009).

9 Cho, N. J., Jackman, J. A., Liu, M. & Frank, C. W. pH-Driven Assembly of Various Supported Lipid Platforms: A Comparative Study on Silicon Oxide and Titanium Oxide. *Langmuir* **27**, 3739-3748, doi:Doi 10.1021/La104348f (2011).

10 Moseke, C. & Ewald, A. Cell and protein adsorption studies using quartz crystal microgravimetry with dissipation monitoring. *Materialwiss Werkst* **40**, 36-42, doi:DOI 10.1002/mawe.200800414 (2009).

11 Kim, J. M., Chang, S. M., Suda, Y. & Muramatsu, H. Stability study of carbon graphite covered quartz crystal. *Sensors and Actuators a-Physical* **72**, 140-147 (1999).

12 Chen, W. Y., Huang, H. M., Lin, C. C., Lin, F. Y. & Chan, Y. C. Effect of temperature on hydrophobic interaction between proteins and hydrophobic adsorbents: Studies by isothermal titration calorimetry and the van't Hoff equation. *Langmuir* **19**, 9395-9403, doi:Doi 10.1021/La034783o (2003).

13 Xie, L. M., Ling, X., Fang, Y., Zhang, J. & Liu, Z. F. Graphene as a Substrate To Suppress Fluorescence in Resonance Raman Spectroscopy. *Journal of the American Chemical Society* **131**, 9890-+, doi:Doi 10.1021/Ja9037593 (2009).

14 So, C. R. *et al.* Molecular Recognition and Supramolecular Self-Assembly of a Genetically Engineered Gold Binding Peptide on Au{111}. *Acs Nano* **3**, 1525-1531, doi:Doi 10.1021/Nn900171s (2009).

15 Ohno, Y., Maehashi, K., Yamashiro, Y. & Matsumoto, K. Electrolyte-Gated Graphene Field-Effect Transistors for Detecting pH Protein Adsorption. *Nano Letters* **9**, 3318-3322, doi:Doi 10.1021/Nl901596m (2009).

16 Castro Neto, A. H., Guinea, F., Peres, N. M. R., Novoselov, K. S. & Geim, A. K. The electronic properties of graphene. *Reviews of Modern Physics* **81**, 109-162, doi:DOI 10.1103/RevModPhys.81.109 (2009).

17 Novoselov, K. S. *et al.* Electric field effect in atomically thin carbon films. *Science* **306**, 666-669, doi:10.1126/science.1102896 (2004).

18 Gong, S. Q. & Yang, M. H. Immunosensor for the detection of cancer biomarker based on percolated graphene thin film. *Chemical Communications* **46**, 5796-5798, doi:10.1039/c0cc00675k (2010).
19 Guo, Y. J. *et al.* Cyclodextrin Functionalized Graphene Nanosheets with High Supramolecular Recognition Capability: Synthesis and Host-Guest Inclusion for Enhanced Electrochemical Performance (vol 4, pg 4001, 2010). *Acs Nano* **4**, 5512-5512, doi:10.1021/nn101860d (2010).
20 Hu, P. A. *et al.* Carbon Nanostructure-Based Field-Effect Transistors for Label-Free Chemical/Biological Sensors. *Sensors* **10**, 5133-5159 (2010).
21 Huang, Y. X. *et al.* Nanoelectronic biosensors based on CVD grown graphene. *Nanoscale* **2**, 1485-1488 (2010).
22 Ohno, Y., Maehashi, K. & Matsumoto, K. Chemical and biological sensing applications based on graphene field-effect transistors. *Biosensors & Bioelectronics* **26**, 1727-1730, doi:10.1016/j.bios.2010.08.001 (2010).
23 Oren, E. E. *et al.* A novel knowledge-based approach to design inorganic-binding peptides. *Bioinformatics* **23**, 2816-2822, doi:DOI 10.1093/bioinformatics/btm436 (2007).
24 So, C. R. *et al.* Controlling Self-Assembly of Engineered Peptides on Graphite by Rational Mutation. *Acs Nano* **6**, 1648-1656, doi:10.1021/nn204631x (2012).
25 Hnilova, M. *et al.* Effect of Molecular Conformations on the Adsorption Behavior of Gold-Binding Peptides. *Langmuir* **24**, 12440-12445, doi:10.1021/la801468c (2008).
26 Charlier, J. C., Eklund, P. C., Zhu, J. & Ferrari, A. C. Electron and phonon properties of graphene: Their relationship with carbon nanotubes. *Top Appl Phys* **111**, 673-709 (2008).
27 Chen, J. H., Jang, C., Xiao, S. D., Ishigami, M. & Fuhrer, M. S. Intrinsic and extrinsic performance limits of graphene devices on SiO2. *Nature Nanotechnology* **3**, 206-209, doi:DOI 10.1038/nnano.2008.58 (2008).
28 Akturk, A. & Goldsman, N. Electron transport and full-band electron-phonon interactions in graphene. *J Appl Phys* **103**, doi:Artn 053702

Doi 10.1063/1.2890147 (2008).
29 Zhu, W., Perebeinos, V., Freitag, M. & Avouris, P. Carrier scattering, mobilities, and electrostatic potential in monolayer, bilayer, and trilayer graphene. *Physical Review B* **80**, 235402 (2009).
30 Adam, S., Hwang, E. H. & Das Sarma, S. Scattering mechanisms and Boltzmann transport in graphene. *Physica E: Low-dimensional Systems and Nanostructures* **40**, 1022-1025, doi:10.1016/j.physe.2007.09.064 (2008).
31 Ferrari, A. C. *et al.* Raman spectrum of graphene and graphene layers. *Physical Review Letters* **97**, -, doi:Artn 187401

Doi 10.1103/Physrevlett.97.187401 (2006).
32 Reina, A. *et al.* Large Area, Few-Layer Graphene Films on Arbitrary Substrates by Chemical Vapor Deposition. *Nano Letters* **9**, 30-35 (2009).
33 Gomez-Navarro, C. *et al.* Electronic transport properties of individual chemically reduced graphene oxide sheets. *Nano Letters* **7**, 3499-3503 (2007).
34 Zhou, M., Zhai, Y. M. & Dong, S. J. Electrochemical Sensing and Biosensing Platform Based on Chemically Reduced Graphene Oxide. *Analytical Chemistry* **81**, 5603-5613, doi:Doi 10.1021/Ac900136z (2009).
35 He, Q. Y. *et al.* Centimeter-Long and Large-Scale Micropatterns of Reduced Graphene Oxide Films: Fabrication and Sensing Applications. *Acs Nano* **4**, 3201-3208 (2010).

36 Dua, V. *et al.* All-Organic Vapor Sensor Using Inkjet-Printed Reduced Graphene Oxide. *Angewandte Chemie-International Edition* **49**, 2154-2157 (2010).
37 Coleman, J. N. *et al.* High-yield production of graphene by liquid-phase exfoliation of graphite. *Nature Nanotechnology* **3**, 563-568, doi:10.1038/nnano.2008.215 (2008).
38 Gamo, Y., Nagashima, A., Wakabayashi, M., Terai, M. & Oshima, C. Atomic structure of monolayer graphite formed on Ni(111). *Surface Science* **374**, 61-64, doi:10.1016/s0039-6028(96)00785-6 (1997).
39 Li, X. S. *et al.* Large-Area Synthesis of High-Quality and Uniform Graphene Films on Copper Foils. *Science* **324**, 1312-1314, doi:10.1126/science.1171245 (2009).
40 Hummers, W. S. & Offeman, R. E. Preparation of Graphitic Oxide. *Journal of the American Chemical Society* **80**, 1339-1339, doi:10.1021/ja01539a017 (1958).
41 Coleman, J. N. Liquid-Phase Exfoliation of Nanotubes and Graphene. *Adv. Funct. Mater.* **19**, 3680-3695, doi:10.1002/adfm.200901640 (2009).
42 Page, T. R., Hayamizu, Y., So, C. R. & Sarikaya, M. Electrical detection of biomolecular adsorption on sprayed graphene sheets. *Biosensors and Bioelectronics* **33**, 304-308, doi:10.1016/j.bios.2012.01.012 (2012).
43 Ishigami, M., Chen, J. H., Cullen, W. G., Fuhrer, M. S. & Williams, E. D. Atomic structure of graphene on SiO2. *Nano Letters* **7**, 1643-1648, doi:10.1021/nl070613a (2007).
44 Girit, C. O. & Zettl, A. Soldering to a single atomic layer. *Applied Physics Letters* **91**, -, doi:Artn 193512

Doi 10.1063/1.2812571 (2007).
45 Kim, S. N. *et al.* Preferential Binding of Peptides to Graphene Edges and Planes. *Journal of the American Chemical Society* **133**, 14480-14483, doi:10.1021/ja2042832 (2011).
46 Wright, A. K. & Thompson, M. R. Hydrodynamic structure of bovine serum albumin determined by transient electric birefringence. *Biophysical Journal* **15**, 137-141, doi:10.1016/s0006-3495(75)85797-3 (1975).
47 Ta, T. C. & McDermott, M. T. Investigation of dual component protein films on graphite with scanning force microscopy. *Colloids and Surfaces B-Biointerfaces* **32**, 191-202, doi:Doi 10.1016/S0927-7765(03)00178-4 (2003).
48 Coleman, J. N. *et al.* Two-Dimensional Nanosheets Produced by Liquid Exfoliation of Layered Materials. *Science* **331**, 568-571, doi:DOI 10.1126/science.1194975 (2011).
49 Jung, L. S. & Campbell, C. T. Sticking probabilities in adsorption from liquid solutions: Alkylthiols on gold. *Physical Review Letters* **84**, 5164-5167 (2000).
50 Sarikaya, M., Tamerler, C., Jen, A. K. Y., Schulten, K. & Baneyx, F. Molecular biomimetics: nanotechnology through biology. *Nature Materials* **2**, 577-585 (2003).
51 Demir, H. V. *et al.* Spatially Selective Assembly of Quantum Dot Light Emitters in an LED Using Engineered Peptides. *Acs Nano* **5**, 2735-2741, doi:10.1021/nn103127v (2011).
52 Sarikaya, M. *et al.* Quartz Binding Peptides as Molecular Linkers towards Fabricating Multifunctional Micropatterned Substrates. *Advanced Materials* **21**, 295-299, doi:10.1002/adma.200801877 (2009).
53 Tamerler, C. *et al.* Directed Self-Immobilization of Alkaline Phosphatase on Micro-Patterned Substrates Via Genetically Fused Metal-Binding Peptide. *Biotechnology and Bioengineering* **103**, 696-705, doi:10.1002/bit.22282 (2009).